D1.1 Labscale properties

Juha Koivisto
Yuki Yamamoto

Grant Agreement Number	101161052
Action Acronym	ARCHIBIOFOAM
Action Title	Digital design and robotic fabrication of biofoams for adaptive mono-material architecture
Funding Scheme	HORIZON-EIC-2023-PATHFINDERCHALLENGES-01
Version date of the Annex I against which the assessment will be made	31/05/2024
Start date of the project	1/10/2024
Due date of the deliverable	30/09/2025
Actual date of submission	30/09/2025
Responsible	AALTO
Contributors	ICD, UMIL, WOAMY
Dissemination level	PUBLIC

European Innovation Council

Funded by the European Union

ARCHIBIOFOAM project has received funding from the European Union's Horizon Europe research and innovation programme under grant agreement No 101161052. Views and opinions expressed are however those of the author(s) only and do not necessarily reflect those of the European Union or European Innovation Council and SMEs Executive Agency (EISMEA). Neither the European Union nor the granting authority can be held responsible for them.

Change Log

Date	Version	Author/Editor	Summary of Changes Made
29/08/2025	V1.0	Yuki Yamamoto (AALTO)	Initial version of the deliverable
16/09/2025	V1.1	Juha Koivisto (AALTO)	Final Version
24/09/2025	V.1.2	Juha Koivisto (AALTO)	Updated table of contents

Executive Summary

Deliverable 1.1 presents the development and characterization results of shape-changing and load-bearing bulk biofoam material intended for meter-scale applications. This report details the systematic engineering approach to creating functional biofoam microstructures with adjustable properties. A comprehensive set of mechanical and thermal characterization data is provided, enabling the parametric model of material property in subsequent work packages.

The structure of biofoam demonstrates responsive behavior to temperature changes, with controlled cyclic deformation achieved through multi-layered structures utilizing materials with varying expansion rates. The report outlines the laboratory-scale production methodology, characterization techniques, and achieved performance metrics for the first generation of functional biofoam samples. These findings provide the foundation for the robotized production process to be developed in later stages of the project. The final data are provided below:

Measurable	Value	Unit
Methylcellulose concentration	1.5	wt%
Fiber concentration	0	wt%
Water concentration	98.5	wt%
Density	17.8	mg/cm3
Young's Modulus	150	kPa
Poisson ratio[1]	-3	%
Size of unit cell	206	cm3
Volume increase per humidity	1.30	cm3/rH
Volume increase per temperature	−0.94	cm3/°C
Volume expansion by humidity	0.6	%/rH
Volume expansion by temperature	-0.5	%/°C

Data in excel format is attached to this document.

[1] Data taken from sample with Methylcellulose wt% 1.5, fiber wt% 1.5 and water wt% 97

Table of Contents

1. Introduction and Objectives

The development of bulk biofoam materials is a central objective of this project, aimed at creating sustainable, shape-changing, and load-bearing solutions for large-scale applications. Deliverable 1.1 contributes to this goal by producing lab-scale samples and generating a structured dataset of their key properties.

The scope of this work covers two main outcomes. First, laboratory samples were manufactured from suspensions containing defined weight percentages of raw materials, prepared under controlled conditions to ensure reproducibility. Second, the samples were systematically characterized with respect to mechanical, hygroscopic, and thermal properties. These data provide the foundation for evaluating material performance and guiding parametric modeling in later stages of the project.

The dataset includes density and Young's modulus as indicators of structural behavior, as well as volume changes linked to humidity and temperature fluctuations. In addition, information on unit cell dimensions and bounding box sizes connects processing parameters with resulting material properties. Together, these results capture the essential physical and environmental responses of the material at this stage of development.

All data are managed according to the project's data management plan and will be published after appropriate intellectual property protection is secured. The results reported here form a baseline for predictive modeling, scale-up, and integration into subsequent work packages.

2. Mechanical Properties

Table 1: Mechanical properties of the foam composition and principle mechanical properties.

MC [%]	Lignin [%]	Graphite [%]	PCC [%]	Citric Acid [%]	ρ [kg/m3]	E_1 [kPa]	STD E_1 [kPa]	E_2 [kPa]	STD E_2 [kPa]	σ_1 [kPa]	σ_1s [kPa.m3/kg]	σ_2 [kPa]	σ_2s [kPa.m3/kg]
1,5	0	0	0	0	19,8	132	42,5	504	99,8	127	6,41	103	5,19
1,5	0,5	0	0	0	26,4	154	26,9	559	145	154	5,86	143	5,43
1,5	1	0	0	0	29,5	134	35,3	543	128	136	4,62	147	4,97
1,5	1,5	0	0	0	34,2	124	13,8	576	97,0	167	4,88	173	5,08
1,5	2	0	0	0	42,7	137	62,3	672	170	156	3,65	243	5,69
1,5	0	0,5	0	0	25,1	246	37,8	791	241	240	9,57	194	7,75
1,5	0	1	0	0	29,4	196	43,8	930	210	276	9,37	228	7,75
1,5	0	1,5	0	0	30,8	241	42,1	991	235	224	7,28	179	5,81
1,5	0	2	0	0	39,8	314	111	879	224	249	6,26	195	4,89
1,5	0	0	0,5	0	22,5	201	34,4	532	108	149	6,63	118	5,24
1,5	0	0	1	0	31,4	129	49,6	788	207	160	5,10	139	4,43
1,5	0	0	1,5	0	35,7	149	63,9	936	165	159	4,45	153	4,28
1,5	0	0	2	0	40,8	189	65,2	1012	269	147	3,61	187	4,58
1,5	0	0	0	0,5	21,2	108	19,8	443	117	77,2	3,65	100	4,71
1,5	0	0	0	1	20,4	154	38,6	728	45,1	90,5	4,44	114	5,57
1,5	0	0	0	1,5	35,6	82	16,9	283	19,9	68,0	1,91	70,8	1,99
1,5	0	0	0	2	27,2	143	39,8	401	133	107	3,94	114	4,20

Mechanical characterization provides the essential baseline for assessing the performance of the developed foam. Three key parameters were selected for evaluation: **density**, **Young's modulus**, and **Poisson's ratio**. Together, these properties describe the structural efficiency, stiffness, and deformation behaviour of the material under load. The results are illustrated in Table 1 with the explanation of columns as:

- **MC [%]:** Weight percent of methylcellulose
- **Lignin [%]:** Weight percent of lignin
- **Graphite [%]:** Weight percent of graphite
- **PCC [%]:** Weight percent of precipitated calcium carbonate
- **Citric Acid [%]:** Weight percent of citric acid
- **ρ [kg/m3]:** Density of the foam
- **E_1 [kPa]:** Average compressive Young's modulus in the weak direction
- **STD E_1 [kPa]:** Standard deviation of compressive Young's modulus in the weak direction
- **E_2 [kPa]:** Average compressive Young's modulus in the strong direction

- **STD E_2 [kPa]:** Standard deviation of compressive Young's modulus in the strong direction
- **σ_1 [kPa]:** Average resulting stress at 80% compressive strain in the weak direction
- **σ_1s [kPa.m3/kg]:** Average specific resulting stress at 80% compressive strain in the weak direction
- **σ_2 [kPa]:** Average resulting stress at 80% compressive strain in the strong direction
- **σ_2s [kPa.m3/kg]:** Average specific resulting stress at 80% compressive strain in the strong direction

2.1 Young's modulus

All mechanical testing was performed using a universal testing machine (Instron E1000). The compressive Young's modulus was determined by applying displacement-controlled compression on cubic samples with approximate dimensions of 30 × 30 × 30 mm. The machine recorded both displacement and the corresponding force. Stress was calculated as the applied force divided by the sample's cross-sectional area, while strain was obtained by dividing the displacement by the sample's initial thickness.

$$\sigma = \frac{F}{A} \text{ and } \varepsilon = \frac{d}{h_0}$$

are the equations that calculate stress (σ) and strain (ε). Where F, A, d, and h_0 denote the force, area, displacement, and the initial height, respectively.

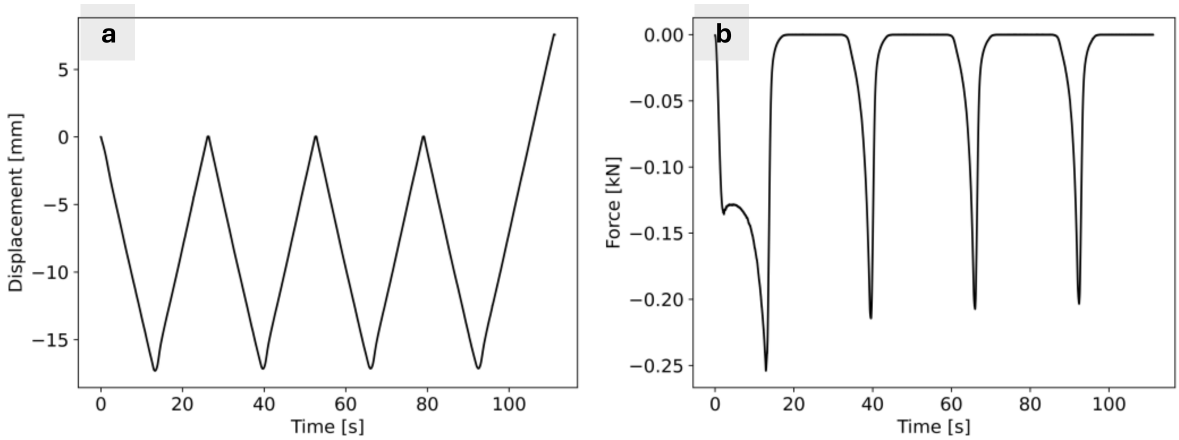

Figure 1. Raw data from one of the experiments which demonstrates the method utilized to obtain the compressive behavior of samples; (a) Displacement-time plot and (b) the resulting force-time plot.

Figure 1 shows the force–time response during displacement-controlled compression. Notice that at certain intervals the recorded force drops to zero. This occurs because the samples were compressed to 70% of their original height at a rate of 80 mm/min, followed by unloading at the same rate. During unloading, the compression plate temporarily loses contact with the sample, resulting in no load detection. This loss of contact arises from permanent damage and viscoelastic effects in the foam: the samples do not fully recover their original dimensions, and any partial recovery occurs at a rate slower than 80 mm/min.

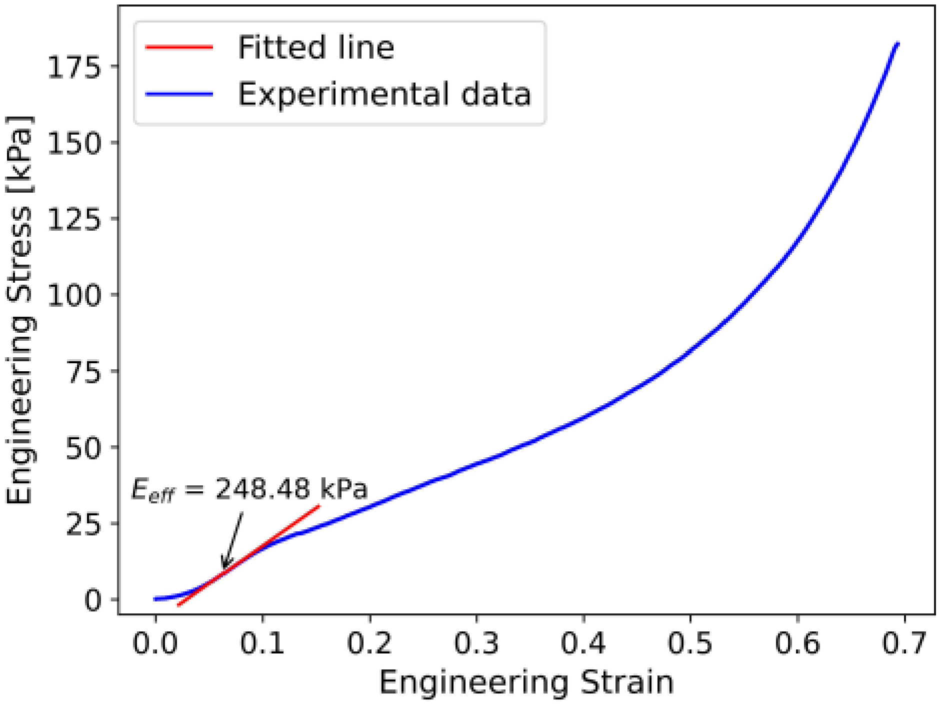

Figure 2. Determination of the Young's modulus from the initial linear fit of the stress-strain response.

The compressive Young's modulus (a measure of sample stiffness) was determined by fitting a straight line to the initial linear portion of the stress–strain curves. Figure 2 presents the stress–strain curve of one representative sample during the first compression cycle. As evident from the figure, the initial region exhibits a well-defined linear response, enabling a reliable estimation of the compression modulus in accordance with the literature.

2.3 Poisson's ratio

Sample Preparation

The test specimen was composed of vertically stacked foam sheets bonded during manufacturing. Due to the natural misalignment of peaks and valleys between layers, structural voids were present throughout the sample. These discontinuities made it impossible to obtain a fully dense structure and directly influenced the selection of Regions of Interest (ROI) for strain analysis.

Digital Image Correlation (DIC) Acquisition

Uniaxial compression tests were performed in the weak direction using an Instron Electropuls E1000 with a 2 kN load cell. A Canon EOS R7 camera equipped with a Canon EF 100 mm f/2.8L Macro IS USM lens and mount adapter was used to capture grayscale images at one-second intervals. The Y-axis corresponded to the loading direction, while the X-axis represented the transverse direction where lateral strain was measured.

DIC Setup

Analysis was conducted with the NCorr MATLAB toolbox. To ensure reliability, two rectangular ROIs were defined within continuous regions of the foam, avoiding areas with voids. The following settings were applied:

- Subset radius: 56 pixels
- Strain radius: 13 pixels
- Subset spacing: 8 pixels
- Image resolution: 2400 × 1600 pixels
- Step analysis: Disabled (single-image mode)

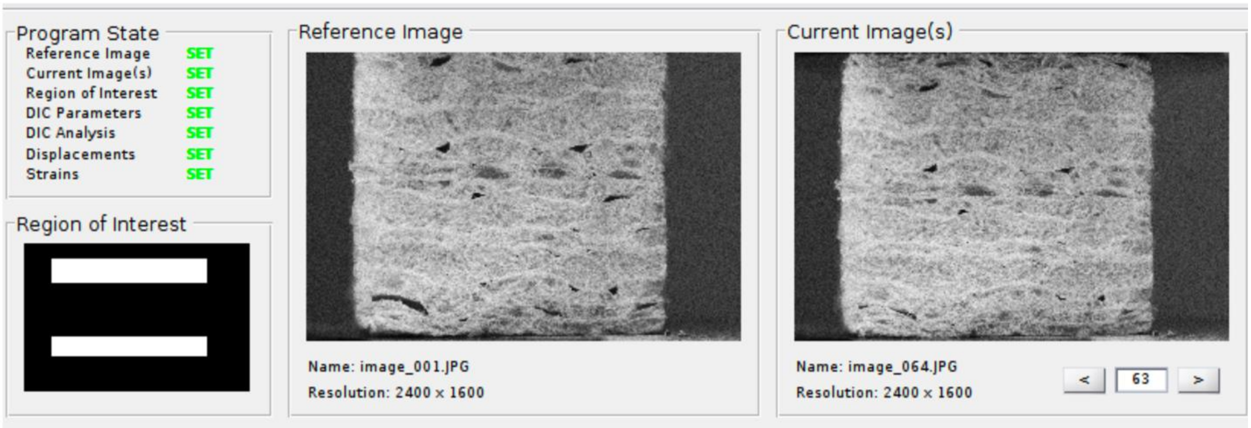

Figure 3. the NCorr interface with the selected ROIs (71st image).

Representative Strain Fields

Figure 3 illustrates the longitudinal and transverse strain maps (ε_{yy} and ε_{xx}) obtained during compression. As expected for porous foams, the strain distribution was heterogeneous. The use of ROIs successfully excluded unreliable regions with structural voids, resulting in consistent strain measurements in the continuous regions of the material.

Poisson's Ratio Evolution

The Poisson's ratio (v) was calculated as:

$$\nu = -\frac{\varepsilon_{xx}}{\varepsilon_{yy}}$$

where ε_{xx} is the transverse strain and ε_{yy} is the axial strain.

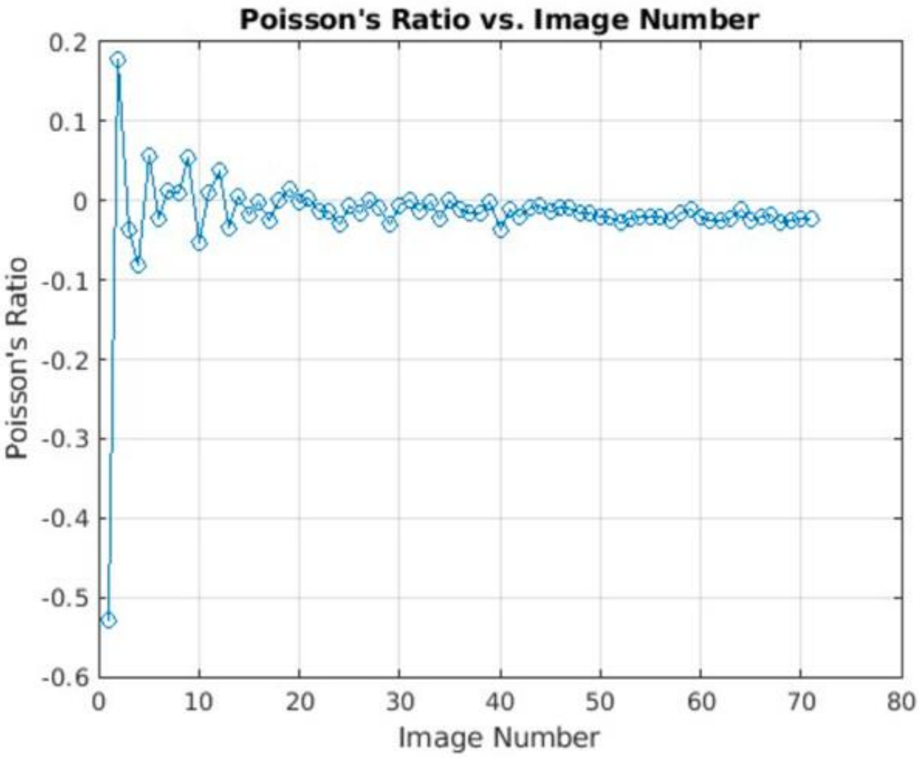

Figure 4. Evolution of Poisson's ratio as a function of image number during uniaxial compression of the foam specimen.

The initial frames (images 1–10) showed large fluctuations caused by noise at low deformation levels. Beyond image 10, ν stabilized around a small negative value, indicating slight lateral contraction under uniaxial compression.

Conclusion

To obtain a representative value, only the stabilized region of the curve (images 11–71) was analyzed. The mean Poisson's ratio was determined to be:

$$\nu = -0.036 \pm 0.0127 = 3 \pm 1\,\%$$

The negative mean value indicates that the foam contracts slightly laterally when compressed in the axial direction. This behavior is consistent with the highly porous structure of the material, where localized collapse and densification reduce the likelihood of significant transverse expansion. The relatively high variability compared to the mean is attributed to material heterogeneity and low overall deformation rather than measurement errors. Overall, these results align with expected mechanical responses of low-density foam structures and provide an important parameter for future modeling of structural performance.

3. Thermal and Moisture expansion

The thermal and humidity expansion properties provide essential information for evaluating the performance of the developed foam under varying environmental conditions. Two key parameters were evaluated spearheaded in this evaluation: volume change per humidity unit [m3/rH] and volume change per temperature unit [m3/°C]. These properties describe how the material responds to changes in moisture levels and temperature, affecting its volumetric stability and overall performance. The raw data is shown in table

Table 2: Shape changes are measured for different samples as radius of curvature. Each sample is conditioned in four humidity-temperature combinations allowing to calculate the volume of the sample in constant humidity (80rH and 15rH) with variable temperature (25C and 50 C) and vice versa.

	ID	Temperature (C)	Humidity (%)	Radius (cm)	Arc length (cm)	chord length (cm)	Thickness (cm)	Width (cm)	volume (cm^3)
small square	1	25	80	13,03	8,5	8,35	0,3	8,5	206
	2	25	15	7,75	8,5	8,08	0,3	8,5	122
	3	50	80	11,57	8,5	8,31	0,3	8,5	183
	4	50	15	6,88	8,5	7,97	0,3	8,5	108
square (worse side)	5	25	80	20,38	10	9,9	0,3	10	381
	6	25	15	12,37	10	9,73	0,3	10	230
	7	50	80	15,62	10	9,83	0,3	10	292
	8	50	15	10,41	10	9,62	0,3	10	193
square (better side)	9	25	80	12,86	10	9,75	0,3	10	240
	10	25	15	7,27	10	9,23	0,3	10	134
	11	50	80	10,41	10	9,62	0,3	10	193
	12	50	15	6,63	10	9,08	0,3	10	122
grid	13	25	80	28,15	12,4	12,3	0,35	12,4	763
	14	25	15	14,02	12,4	12	0,35	12,4	378
	15	50	80	20,4	12,4	12,21	0,35	12,4	552
	16	50	15	13,06	12,4	11,94	0,35	12,4	351
diagonal grid	17	25	80	25,32	11	10,9	0,35	11	608
	18	25	15	15,15	11	10,76	0,35	11	362
	19	50	80	18,02	11	10,83	0,35	11	432
	20	50	15	14,84	11	10,75	0,35	11	355
3%mC Square	21	25	80	5,78	9,7	8,6	0,4	9,7	136
	22	25	15	4,34	9,7	7,8	0,4	9,7	101
	23	50	80	5,41	9,7	8,45	0,4	9,7	127
	24	50	15	4,14	9,7	7,63	0,4	9,7	96
Elongated grid	25	25	80	34,88	11,4	11,3	0,35	11,4	866
	26	25	15	24,65	11,4	11,25	0,35	11,4	611
	27	50	80	34,88	11,4	11,3	0,35	11,4	866
	28	50	15	22,5	11,4	11,23	0,35	11,4	557
Even grid	29	25	80	22,6	8,5	8,45	0,3	8,5	360
	30	25	15	16,83	8,5	8,41	0,3	8,5	267
	31	50	80	20,63	8,5	8,44	0,3	8,5	328
	32	50	15	14	8,5	8,37	0,3	8,5	222
Double grid	33	25	80	10,14	10	9,6	0,6	10	371
	34	25	15	6,95	10	9,16	0,6	10	251
	35	50	80	9,67	10	9,56	0,6	10	353
	36	50	15	6,6	10	9,07	0,6	10	238
Grid (paper)	37	25	80	11,73	10	9,7	0,35	10	254
	38	25	15	7,93	10	9,35	0,35	10	171
	39	50	80	10,28	10	9,61	0,35	10	222
	40	50	15	7,58	10	9,29	0,35	10	163

3.1 Hygroscopic properties

The hygroscopic behavior of the foam was investigated through curvature testing, in which samples were subjected to controlled humidity cycles at constant temperature. The material's response was evaluated by monitoring dimensional changes and curvature development of the foam layer fixed on a mesh base. (Figure 5) These changes result from the foam's intrinsic expansion and contraction when exposed to varying relative humidity (RH) levels.

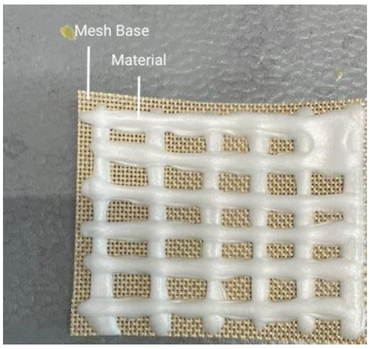

Figure 5. Example of foam and mesh (sample to test humidity and temperature reaction on grid pattern

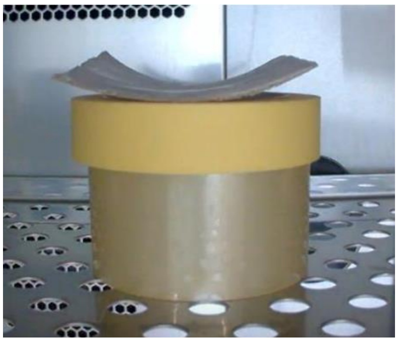

Figure 6. Example image of experiments set-up

In the current setup, humidity cycles consisted of alternating phases at 25 °C and 80 % RH, and 25 °C and 15 % RH, with each phase lasting 4 hours and 30 minutes. The radius of curvature for each state was calculated from measured chord and arc lengths using a custom Python script. To minimize measurement error, chord lengths were obtained immediately after removing the sample from the humid environment, as the foam begins to relax rapidly once exposed to ambient air.

Although only preliminary tests have been conducted, the results already indicate a clear correlation between humidity changes and foam curvature. Most notably, the foam exhibited a volume change per humidity unit of 1.30 cm^3/rH for a sample of size 206 cm3. A dimensionless volume change is $\boldsymbol{c_{hum}}$ **= 0.6 %/rH** which is a key quantitative measure of its hygroscopic sensitivity. Higher humidity levels induce expansion, leading to increased curvature, while lower humidity levels cause contraction. In addition, layer structuring strongly influences the response: when multiple foam layers are deposited sequentially, the most recently applied layer dominates the direction of curvature. Differences in local density within the same pattern also lead to asymmetric bending, as observed in 10×10 square structures where the less compact side exhibited reduced curvature. These findings demonstrate the foam's strong hygroscopic sensitivity and underline the importance of pattern design and material density distribution in controlling dimensional changes under varying environmental conditions.

3.2 Temperature-related properties

Temperature effects on the foam were studied through combined thermal-humidity cycles. Samples were exposed to alternating phases of 25 °C at 80 % RH and 50 °C at 15 % RH, with each phase lasting 4 hours and 30 minutes. A second series of tests maintained constant humidity (80 % RH) while varying the temperature between 25 °C and 50 °C. Curvature was again determined through chord and arc length measurements analyzed with the same computational method used for humidity testing.

The results confirm that temperature changes significantly affect the foam's dimensional stability. A volume change per temperature unit of −0.936 cm^3/°C for a sample of size 206 cm3 was recorded leading to dimensionless expansion constant of c_{temp} **= -0.4 %/°C**, indicating that increasing the temperature consistently caused shrinkage and thus higher curvature. Increasing the temperature caused shrinkage of the foam, producing higher curvature. (Figure 7). When humidity was kept constant, the thermal response was still pronounced, indicating that temperature alone plays a key role in the material's expansion–contraction mechanism.

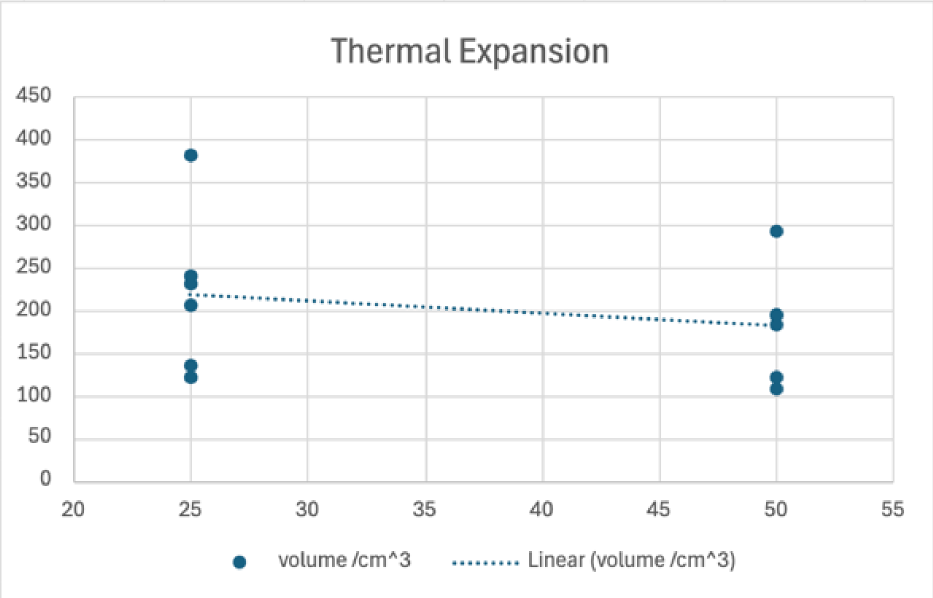

Figure 7. Thermal expansion between 25 °C and 50 °C

As with humidity tests, the structural configuration of the foam influenced the observed curvature. Samples with weak or porous structures displayed smaller bending radii, while multilayered patterns showed anisotropic behavior dictated by the orientation of the topmost layer. These effects highlight the coupled influence of processing design and environmental stimuli on the foam's performance.

Overall, the foam demonstrates a reversible and predictable thermo-responsive behavior, making it a promising candidate for applications where controlled shape-change under environmental fluctuations is desirable. Further testing with a larger sample set will refine the quantitative expansion coefficients and support integration into predictive material models.

4. Conclusion and Future Directions

Lab-scale biofoam samples were produced and characterized for their mechanical and environmental response. Key results include:

- **Young's modulus:** 150 kPa
- **Poisson's ratio:** −3 ± 1 %
- **Volume change per humidity:** 0.6 %/rH
- **Volume change per temperature:** -0.4 %/°C

These results demonstrate the foam's strong responsiveness to environmental conditions, with density distribution, fiber structuring, and pattern design influencing curvature behavior.